APPLICATION OF CLOSED-FORM SOLUTIONS TO A MESH POINT FIELD IN SILICON SOLAR CELLS

M. F. Lamorte
Research Triangle Institute
Research Triangle Park, NC 27709

Abstract

A computer simulation method will be discussed that provides for equivalent simulation accuracy, but that exhibits significantly lower CPU running time per bias point compared to other techniques. This new method is applied to a mesh point field as is customary in numerical integration (NI) techniques. The assumption of a linear approximation for the dependent variable, which is typically used in the finite difference and finite element NI methods, is not required. Instead, the set of device transport equations is applied to, and the closed-form solutions obtained for, each mesh point. The mesh point field is generated so that the coefficients in the set of transport equations exhibit small changes between adjacent mesh points. In contrast to the NI linear approximation, the closed-form solutions more accurately represent the physical system and the device physics incorporated in the transport equations.

Application of this method to high-efficiency silicon solar cells is described; and the method by which Auger recombination, ambipolar considerations, built-in and induced electric fields, bandgap narrowing, carrier confinement, and carrier diffusivities are treated. Bandgap narrowing has been investigated using Fermi-Dirac statistics, and these results show that bandgap narrowing is more pronounced and that it is temperature-dependent in contrast to the results based on Boltzmann statistics. It is also suggested that carrier diffusivity relationships that apply to degenerate materials in thermal equilibrium may also be applicable to regions in which high injection exists even in nondegenerate material.

Imposing the appropriate boundary conditions on the closed-form solutions results in a set of equations which require simultaneous solution. This results in obtaining the solution of all constants of integration, from which, in principle, all cell characteristics may be derived. It has been demonstrated that recursion relationships exist between the constants of integration. Trial or "guess" solutions are not required in this new method for devices operating at any injection level, because the closed-form solutions obtained at each mesh point, in fact, fulfill this role. This carries over to those devices operating at high injection levels, but the inclusion of Auger recombination introduces nonlinear terms in the continuity equations, and special attention must be devoted to satisfying Poisson's equation. Under these conditions, an initial estimate must be made of the value of the independent variable for inclusion in the continuity equations at the initial mesh point. An iterative procedure is then used to obtain a consistent solution.

INTRODUCTION

Computer modeling simulations have been shown to be very useful in the development of semiconductor devices in those cases where the simulation is an accurate representation of the physical device. However, to be an effective aid to the experimentalist and to become an equal partner in the technologies used in device development, it may be required to operate the computer program frequently each day in an active developmental program. For frequent use, as required in solar cell development, CPU costs must be low. Moreover, low CPU cost allows for engaging in computer experiments, which can be made to be a very useful and powerful technique.

Computer modeling using numerical integration (NI) methods in Si device technology have usually shown fair-to-good agreement with experimental data. However, CPU costs for the execution of computer programs that are based on numerical integration methods are prohibitively high for their use as a laboratory or manufacturing tool [1]. The number of bias points that are required to study optimized device designs usually exceeds 5,000 runs. Similarly, a comprehensive study involving device structures or new types of devices may exceed 10,000 runs. Increased CPU cost results if convergent problems arise. In most cases, the cost of such studies, for the benefits gained, may not be attractive.

Simulation accuracy is determined by both the accuracy of the algorithm/analytical method representing the device transport equations, and the accuracy of the phenomena submodels in representing the corresponding experimental data related to material properties. For most efficient use of the CPU, the accuracy of the algorithm/analytical method and of the phenomena submodels should be commensurate. For example, even if the algorithm/analytical method accurately represents the device, simulation results may not agree with experimental data if the phenomena submodels are accurately represente The reverse is also true. In solar cells, the phenomena submodels that produce first-order effects in terminal characteristics are: absorption curve, built-in and induced electric fields, bandgap, lifetime, mobilities, diffusivities, photoexcited carrier concentrations, surface recombination velocities, junction transport, etc. The representation of the phenomena submodels must take on an importance equal to the analytical method used to represent the system.

Under some operating conditions and for a number of solar cell structures, two-dimensional modeling may be required to obtain improved agreement between simulation results and experimental data. Although the results presented above apply generally to one- and two-dimensional modeling, the CPU execution time is significantly greater for two-dimensional simulations.

In this paper, a new method is described which has been used to simulate semiconductor device characteristics. Although this method shares similarities with some aspects of NI methods, it differs markedly in other aspects. Abbreviated forms of analytical relationships representing the solution of solar cell transport equations that are obtained using this new method are presented and discussed. The similarities and differences between the methods are also discussed.

SIMULATION METHODS

In this section, the transport equations are discussed as they relate to the simplifications and approximations that are required to be made in order to use NI methods and the new method, which is the application of closed-form solutions applied to a mesh point field. The finite difference (FD) and finite element (FE) methods, which are considered NI methods, are briefly discussed because they are most similar to this new method. An outline of these methods is presented and the procedures are developed to apply them.

Numerical Integration Methods

The most commonly used transport model in semiconductor devices is due to Van Roosbroeck and is represented by the set of equations:

$$\frac{\partial n}{\partial t} = \frac{1}{q} \nabla \cdot \vec{J}_n + (G-R) \quad , \tag{1}$$

$$\frac{\partial p}{\partial t} = -\frac{1}{q} \nabla \cdot \vec{J}_p + (G-R) \quad , \tag{2}$$

$$\vec{J}_n = q\mu_n n\vec{E} + qD_n \nabla n \quad , \tag{3}$$

$$\vec{J}_p = q\mu_p p\vec{E} - qD_p \nabla p \quad , \tag{4}$$

$$\nabla \cdot \vec{E} = \frac{q}{\epsilon} (p-n + N_D - N_A) \tag{5}$$

The above set of relationships is applicable to nondegenerate and degenerate materials, low and high injection levels, dc and ac operation, and to most semiconductor device structures.

The Van Roosbroeck transport equations comprise a system of coupled partial differential equations that describe a semiconductor carrier concentration and current density in position and time. The net balance of generation sources and recombination sinks of electrons and holes are described by the respective continuity equations, and the Poisson equation describes the electric field distribution that is produced by the charge distributior within the semiconductor. For solar cells, the steady-state condition is assumed, which greatly simplifies the transport set because $\partial n/\partial t$ and $\partial p/\partial t$ vanish. Device phenomena submodels may be added to the transport equations to accurately describe a variety of carrier dynamical and other internal physical processes.

However, the Van Roosbroeck equations must be significantly modified in order to describe the effects arising from velocity overshoot, ballistic transport, and very thin surface layers [3]. In solar cells, only the latter may need consideration. The phenomenon in thin n-type surface layers, where an oxide charge insulator (OCI) produces an electron accumulation, may introduce sidebands within the conduction band, where each sideband corresponds to a quantized level for electron transport in a direction normal to the surface.

Solution of the transport equations is more difficult for higher order models; i.e., time-dependent requirements, and two- and three-dimensional geometries [2-11]. Moreover, this difficulty is brought into sharp focus in two-dimensional modeling when comprehensive phenomena submodels are considered [2,12].

In comprenensive representations, the complexity of the Van Roosbroeck transport equations does not allow for closed-form solutions which accurately simulate semiconductor devices. Accurate solution of the transport equations requires a method that simplifies these equations. The most popular approach is to divide the device structure into small parts [2-15]. In one-, two-, and three-dimensional solutions, these small parts are defined as infinite slabs, areas, and volumes, respectively. Each of these small parts is assigned a mesh point, which is identified by one, two, or three indices corresponding to a one-, two-, or three-dimensional representation of the device. These small parts must be made sufficiently small so that all dependent variables in the transport equations exhibit small changes in value between adjacent mesh points [2,4,5,8, 15]. In addition, the coefficients in the transport equations also exhibit small or negligible changes between adjacent mesh points [15]. If either of these conditions is not met, a solution is not obtained because convergence does not occur. NI methods and the closed-form solutions may be applied to mesh point fields.

In applying the FD method, all derivatives are replaced by finite differences between discrete points in an active domain in the interior of the structure. The residue of the newly established difference equation is set to zero at each mesh point. Thus, the differential equations are transformed into difference operator equations. The value of the dependent variable is determined at each mesh point from the set of equations obtained [2,4].

For example, the differential equation to determine the temperature distribution is given by [4]

$$\frac{d^2T}{dx^2} = 0 \quad . \tag{6}$$

The difference operation is represented by

$$\frac{d^2T}{dx^2} = \frac{\dfrac{T_{i+2} - T_{i+1}}{\Delta x} - \dfrac{T_{i+1} - T_i}{\Delta x}}{x} \quad , \tag{7}$$

where T_i, T_{i+1}, and T_{i+2} are the values of the dependent variable, T, at the mesh points i, i+1, and i+2, and Δx is the independent variable representing the separation of the mesh points i and i+1, and i+1 and i+2, assumed to be equal. A corresponding equation is constructed at each mesh point. The resultant set of equations requires the simultaneous solution for T_1, T_2, --, T_i, --. Thus, the value of the dependent variable, T, is obtained only at the mesh points 1, 2, --, i, --. The value for T in the region between the mesh points is not

obtained explicitly and may only be approximated by one of the established methods. Typically, a linear approximation is used.

In the FE method, a typical assumption made is that the dependent variable is a linear function, where, for the system discussed above involving temperature [4],

$$T = T_i + \frac{T_{i+1} - T_i}{x_{i+1} - x_i} (x - x_i) \quad . \tag{8}$$

This relationship is substituted into an equation, called the "functional," that describes the system to obtain a set of equations. Simultaneous solution of this set results in discrete values of the dependent variable at each of the mesh points. Between the mesh points, the dependent variable is governed by a linear relationship similar to that represented in Eq. (8).

The full numerical solution of partial differential equations as described above, which is applied to a physical system and which describes all regions of this system in a unified manner, was first suggested by Gummel [5]. In this work, Gummel applied his method to a one-dimensional bipolar transistor. Subsequently, the method was further developed by DeMari [6,7] who applied it to p-n junctions, and by Scharfetter and Gummel [8] to IMPATT diodes. Although this initial work was confined to one-dimensional structures, the Gummel approach has also been adapted to two-dimensional modeling [3,9-12]. However, the two-dimensional algorithm requires excessive CPU execution time [3,12].

Phenomena submodels may be imposed on the coupled nonlinear partial differential equations which may result in nonlinear transport equations; i.e., band-to-band Auger recombination introduces a term involving n^2 or p^2, and the electric field in the quasi-neutral region depends on the injection level. In NI numerical methods, the transport relationships are linearized. Two schemes have been used and both require initial "guess" solutions. The decoupled method proposed by Gummel [5] is to assume the coupling is weak so that the equations are solved serially. While the method is not difficult to implement, it fails to give accurate results for highly nonlinear systems. The coupled method, proposed by Hachtel et al. [14], solves the transport equations simultaneously. However, this is more difficult to implement. The implementation of the algorithm becomes complex when recombination-generation and electric field drift terms are included [4]. In addition, this results in significantly higher CPU execution time and increased main memory requirements.

As discussed above, solving NI methods results in values for the dependent variables, such as the carrier concentrations and electric field, at discrete points in the semiconductor; i.e., at the mesh points. Thus, the continuum of the dependent variables, described by the transport equations, is transformed into a discontinuous or discrete set of values representing these variables at each of the mesh points. In contrast, the method that is proposed in this paper does not resort to this transformation.

Closed-form Solutions Applied to a Mesh Point Field

The major point of departure between the algorithms of the new method and NI methods is that the new method uses a closed-form solution which is applied to a mesh point field that defines the system in space and in time [15]. This requires the application of the transport equations to each mesh point. In order to obtain a closed-form solution to the transport equations, the mesh point field is generated so that the equations accurately represent each mesh point. The closed-form relationships represent analytical solutions and result in a continuum of values for the dependent variables in the region between adjacent mesh points. Analytical solutions of adjacent mesh points also provide a continuum of values for the dependent variables in their corresponding regions. Analytical solutions of neighboring mesh points satisfy the usual boundary conditions that are demanded in semiconductor devices in accordance with the electronic/optical model under consideration. The analytical solutions representing the dependent variables at each mesh point contain constants of integration, which are determined by imposing the boundary conditions on each of the solutions.

A procedure has been established in applying the closed-form solutions to a mesh point field. The procedure is as follows [15]: (1) establish the electronic/optical model of the solar cell within the generic transport equations; (2) impose the phenomena submodels, represented in analytical or tabular form, on the transport equations; (3) develop mesh point field distribution of order f which reduces the complexity of, and makes the coefficients that are present in, the continuity equations constant or nearly constant, so that a closed-form solution is obtained at each mesh point with minimum restrictions; (4) establish 2f-boundary conditions on the mesh point field; (5) apply the 2f-boundary conditions on the f-closed-form solutions; and (6) solve the resultant 2f-equations simultaneously to obtain the 2f-constants of integration through recursion relationships. In principle, the transport equations are uniquely and completely solved after the relationships for the 2f-constants of integration are obtained. Electron current is calculated at the depletion region edge; the hole current is determined by a similar relationship. Adding the electron and hole currents results in the J-V relationship from which most of the terminal characteristics are recovered.

The well-established solar cell electronic/optical model is imposed on the transport equations; i.e., optical pair generation of carriers, and minority carrier collection and transport across a p-n junction. This is followed by imposing the phenomena submodels which are subsequently discussed. A mesh point distribution is established so that the electric field, lifetime, mobility, diffusivity, absorption coefficient, and bandgap exhibit small changes between adjacent mesh points. Figure 1 shows the subdivision of a one-dimensional solar cell structure. The n-region $(0, X_2)$ and the p-region (X_3, X_5) are subdivided into f_n- and f_p-mesh points, respectively. To illustrate the method, the p-region transport solution is discussed below. The electron continuity equation is represented by

$$\int_0^{\lambda_c} \alpha N_0 \exp\left(-\int_0^x \alpha dx'\right) d\lambda + D_n \frac{d^2 n_{pe}(x)}{dx^2} + \mu_n E_p \frac{dn_{pe}(x)}{dx} - \frac{n_p(\cdot) - n_{p0}}{\tau_n} = 0 \ , \quad (9)$$

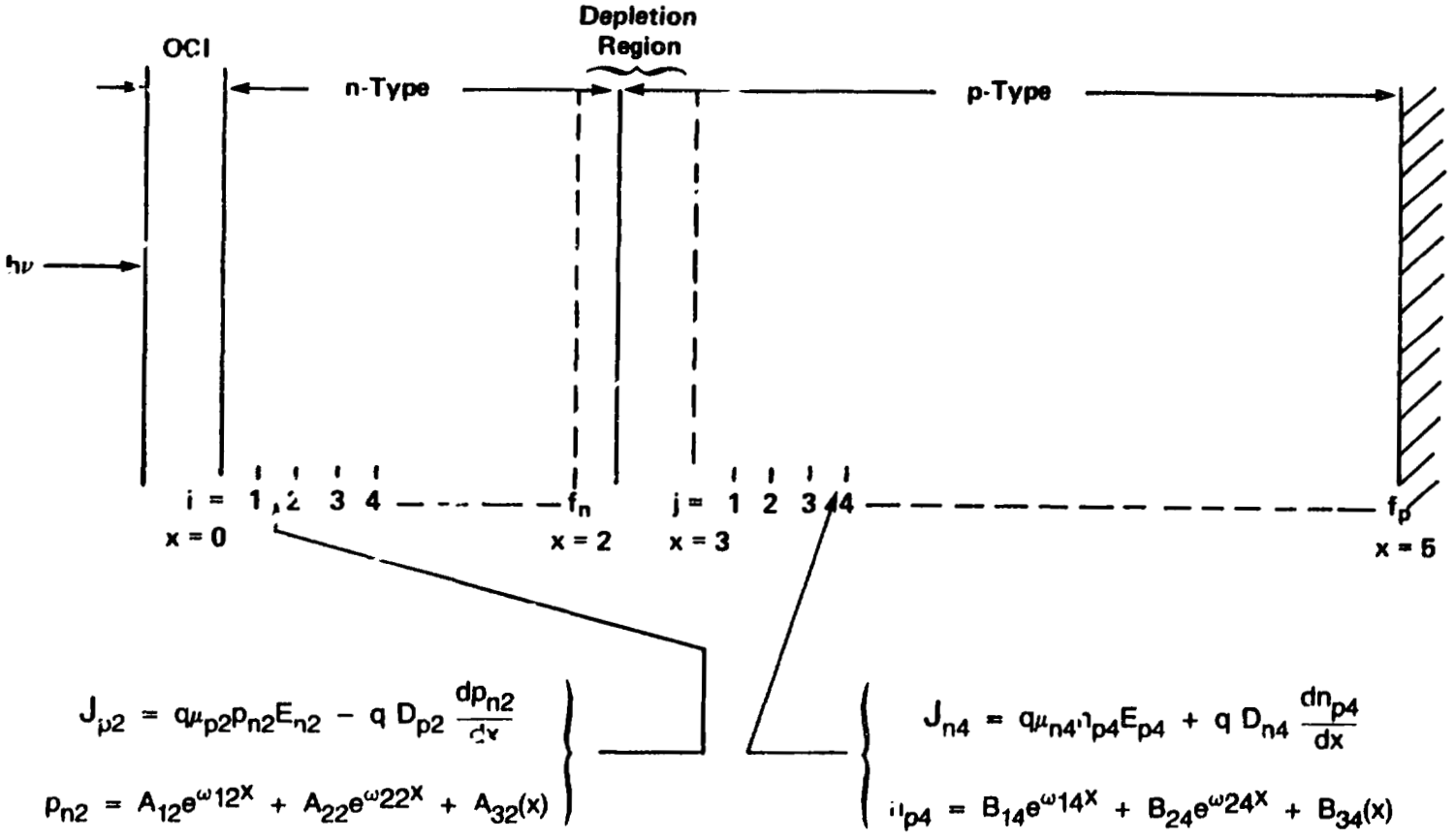

Figure 1. Discretization of 1-dimensional solar cell structure.

where the Poisson equation takes its usual form. The symbols have their usual definitions, where n_p and n_{pe} represent the total and photoexcited electron concentrations, respectively. Implicit in Eq. (9) is that the subdivision results in a condition in which the slope of the electric field, dE_p/dx, is small and may be neglected in a region between adjacent mesh points. Although the electric field slope is assumed to be negligible, the electric field itself, in general, is allowed to vary from mesh point to mesh point. Moreover, under these conditions the remaining material properties also exhibit small changes between neighboring mesh points for low injection levels. These changes become large under high injection levels, in which case a more dense mesh point field may be required to maintain comparable changes. As a result, a near-exact closed-form solution is obtained at each mesh point for the photoexcited electron concentration, which is an exact solution of Eq. (9) and is represented by

$$n_{pej}(x) = B_{1j}\exp(\omega_{1j}x) + B_{2j}\exp(\omega_{2j}x) + B_{3j}(x) \quad , \qquad (10)$$

where the terms comprising Eq. (10) are given in Table 1.

The subscripts, j, in Eqs. (10)-(30) represent the j^{th} mesh point in the p-region as indicated in Figure 1. Correspondingly, in Eq. (10), B_{1j} and B_{2j} represent the constants of integration, and B_{3j} in Eq. (11) represents the photoexcited electron concentration, produced by photon absorption in the region of the j^{th} mesh point. In the context of the conditions imposed on the continuity equations at each mesh point, ω_{1j} and ω_{2j} in Eq. (14) are constants. Photoexcited electron concentration, Eq. (10), is governed by the exponential terms and B_{3j} which are all functions of position; in addition, B_{3j} is also a function of wavelength through Eqs. (12) and (13). Eq. (10) provides for continuous values of n_{pe} through the assignment of values to x, where the range of x is restricted to the region between the (j-1) and j mesh points. In contrast to numerical integration methods, the continuum of values describing the behavior of n_{pe} is preserved in the closed-form scheme as was the original intent proposed by the Van Roosbroeck concept related to the use and the interpretation of the transport equations.

It is clear that the relationship used in the closed-form method, to represent the photoexcited electron concentration, Eq. (10), is an analytical solution that is demanded by, and has its support in, the transport equations. Moreover, this relationship may also incorporate a comprehensive set of phenomena submodels as dictated by the transport equations, imposed boundary conditions, and the representations of the material properties coupled with the mesh point field. The phenomena submodels that influence Eq. (10) are represented in the relationships for the parameters, Eq. (11)-(30), that describe their behavior in the region bounded by the (j-1) and j planes in Figure 1. Eqs. (11)-(13) describe the photon absorption generation rate and the redistribution of the photoexcited electron-hole pairs, while Eq. (14) governs the electron effective diffusion length in the presence of an electric field. Drift and diffusion components of the electron current are represented in Eq. (15), and the electric field used in

Table 1. List of relationships of terms appearing in the solution of the electron concentration, Equation (10).

$$B_{3j}(x) = \frac{1}{\omega_{2j} - \omega_{1j}} [G_{1j}(x)\exp(\omega_{1j}x) + G_{2j}(x)\exp(\omega_{2j}x)] \tag{11}$$

$$G_{1j}(x) = \frac{1}{D_{nj}} \int_o^x \exp(-\omega_{1j}x') \int_o^{\lambda_c(x')} \alpha_j N_{0j} \exp(-\int_o^{x'} \alpha_j dx'')d\lambda dx' \tag{12}$$

$$G_{2j}(x) = -\frac{1}{D_{nj}} \int_o^x \exp(-\omega_{2j}x') \int_o^{\lambda_c(x')} \alpha_j N_{0j} \exp(-\int_o^{x'} \alpha_j dx'')d\lambda dx' \tag{13}$$

$$\left.\begin{matrix}\omega_{1j} \\ \\ \omega_{2j}\end{matrix}\right\} = -\frac{\mu_{nj}E_{pj}}{2D_{nj}} \pm \sqrt{\left(\frac{\mu_{nj}E_{pj}}{2D_{nj}}\right)^2 + L_{nj}^{-2}} \tag{14}$$

$$J_{nj} = q\mu_{nj}n_{pj}E_{pj} + qD_{nj}\frac{dn_{pj}}{dx} \tag{15}$$

$$E_{pj} = E_{p\Omega j} + E_{pBNj} + E_{plPj} + E_{pPEj} \quad , \tag{16}$$

where

$$E_{p\Omega j} = \frac{b_{pj}J_1}{q\mu_{nj}\Gamma_{pj}} \quad , \tag{17}$$

$$E_{pBNj} = (b_{pj} - \xi_p)\frac{n_{poj}}{\Gamma_{pj}} E_{pBNoj} \quad , \tag{18}$$

$$E_{pBNoj} = -\frac{kT}{q}\frac{2}{n_{iej}}\frac{dn_{iej}}{dx} \quad , \tag{19}$$

Table 1 (continued).

$$E_{pIPj} = \left[(b_{pj} - \xi_p) \frac{n_{poj}}{\Gamma_{pj}} + \xi_p \frac{N_{Aj}}{\Gamma_{pj}} \right] E_{pIPoj} \quad , \tag{20}$$

$$E_{pIPoj} = \frac{kT}{q} \frac{1}{N_{Aj}} \frac{dN_{Aj}}{dx} \quad , \tag{21}$$

$$E_{pPEj} = - \frac{kT}{q} \frac{b_{pj} - \xi_p}{\Gamma_{pj}} \frac{dn_{pej}}{dx} \quad , \tag{22}$$

$$\Gamma_{pj} \equiv (b_{\mu j} + \xi_p) n_{pj} + \xi_p N_{Aj} \quad , \tag{23}$$

$$b_{nj} = \frac{F_{1/2}(\eta_j)}{F_{-1/2}(\eta_j)} \tag{24}$$

$$b_{pj} \equiv \frac{F_{1/2}(-\varepsilon_{Gj} - \eta_j)}{F_{-1/2}(-\varepsilon_{Gj} - \eta_j)} \tag{25}$$

$$b_{\mu j} \equiv \frac{\mu_{nj}}{\mu_{pj}} \tag{26}$$

$$D_{nj} = \frac{kT}{q} \mu_{nj} b_{nj} \tag{27}$$

$$J_1 = J_n(x) + J_p(x) \tag{28}$$

$$n_{iej}^2(T, N_A) = n_{io}^2(T) e^{\Delta E_G / kT} \tag{29}$$

$$n_{pj} = n_{poj} + n_{pej} \tag{30}$$

the drift term is given by Eq. (16). The electric field components are defined in Eqs. (17)-(27), arising under equilibrium and nonequilibrium conditions, and include effects produced by ohmic voltage drops in the quasi-neutral regions, bandgap narrowing, impurity concentration profile, and photoexcited electron concentration distribution. Eq. (29) describes the intrinsic concentration with respect to temperature and bandgap narrowing.

In contrast, the relationship that is used in NI methods, corresponding to Eq. (10), is typically linear and is of the form given by

$$n_{pe}(x) = n_{pe}(x_{j-1}) + \frac{n_{pe}(x_j) - n_{pe}(x_{j-1})}{x_j - x_{(j-1)}} (x - x_{(j-1)}) , \qquad (31)$$

where x is the independent variable in the region bounded by the (j-1) and j planes. The photoexcited carrier concentrations, n_{pej} and $n_{pe(j+1)}$, do not normally represent algebraic expressions, but represent discrete values and require initial estimates of the concentrations at their designated positions. The richness of Eq. (10) and its associated parameters, defined in Eqs. (11)-(30), in representing device physics is clearly evident in contrast to the representation in Eq. (31). This relationship, Eq. (31), is used in NI methods because it simplifies the matrix equation that requires solution, but it is artifical in its representation of the photoexcited electron concentration because it has been constructed independent of the transport equations.

The difference in the results obtained by applying Eqs. (10) and (31) to the same mesh point distribution, which defines the solar cell structure, is significant. Applying Eq. (10) results in the determination of the constants of integration, B_{1j} and B_{2j}, assigned to the carrier analytical relationship at each mesh point. Substituting B_{1j} and B_{2j} in Eq. (10) provides for an analytical relationship at each mesh point, describing the behavior of n_{pej} for a continuum of values of x in the range $x_{(j-1)}$ and x_j. In contrast, the results of applying Eq. (31) is a set of discrete values for n_{pej} at each mesh point.

In the work reported in this paper, the general case is treated as it relates to injection level. The information of injection level is contained in the electric field and its components, Eqs. (16)-(30), lifetime through the diffusion length, L_n, and boundary conditions at the depletion edges bounding the p-n junction, and in the carrier mobilities and diffusivities. Application of Eq. (10) requires negligibly small changes in electric field between adjacent mesh points. Under these conditions, Eq. (10) is an excellent approximation to the exact solution at the designed mesh point region. The measure for which Eq. (10) approaches the exact solution is the self-consistency obtained from the solution of the Poisson equation using the analytical relationships for n_{pej} and the number of iterations required to obtain values of B_{1j} and B_{2j}.

The f_p-mesh point distribution in the p-type region of the solar cell comprises $(f_p - 1)$ internal boundaries, and external boundaries at x_3 and x_5. At the external boundaries, the usual p-n junction boundary condition on minority

carrier concentration applies. At each of the (f_p-1) internal boundaries, the electron concentration and electron current, separately, are continuous and are represented by

$$n_{pej}(y_{oj}) = n_{pe(j+1)}(0)k_j \tag{32}$$

where

$$k_j = e^{\Delta Ecj/kT} \tag{33}$$

and

$$J_{nj}(y_{oj}) = J_{n(j+1)}(0) \quad , \tag{34}$$

where y_{oj} is the separation between the $(j-1)^{th}$ and j^{th} mesh points. A surface recombination velocity boundary condition is imposed at the x_5 boundary. This results in $2f_p$-boundary conditions, from which $2f_p$-equations are obtained that must be solved simultaneously to obtain the solution of the $2f_p$-constants of integration.

Applying the boundary conditions using Eqs. (10) and (15) results in $2f_p$-equations which are represented in matrix form by

$$\begin{bmatrix} 1 & 1 & 0 & 0 & 0 & & & & & & & \\ \sigma_1 k_1 & \tau_1 k_1 & -1 & -1 & 0 & & & & & & & \\ \delta_1\sigma_1 & \epsilon_1\tau_1 & -\delta_2 & -\epsilon_2 & 0 & & & & & & & \\ 0 & 0 & \sigma_2 k_2 & \tau_2 k_2 & -1 & -1 & & & & & & \\ 0 & 0 & \delta_2\sigma_2 & \epsilon_2\tau_2 & -\delta_3 & -\epsilon_3 & & & & & & \\ & & & & & & \sigma_i k_i & \tau_i k_i & -1 & -1 & & \\ & & & & & & \delta_i\sigma_i & \epsilon_i\tau_i & -\delta_{i+1} & -\epsilon_{i+1} & & \\ & & & & & & & & & & \sigma_{i_p}[\delta_{i_p}+S_n] & \tau_{i_p}[\epsilon_{i_p}+S_n] \end{bmatrix} \begin{bmatrix} B_{11} \\ B_{21} \\ B_{12} \\ B_{22} \\ B_{13} \\ B_{23} \\ \vdots \\ B_{2i} \\ B_{1(i+1)} \\ \vdots \\ B_{2i_p} \end{bmatrix} = \begin{bmatrix} n_{pe}(x_3) \\ F_{01} \\ F_{02} \\ F_{03} \\ F_{04} \\ F_{05} \\ \vdots \\ F_{0(2i-1)} \\ F_{0(2i)} \\ \vdots \\ F_{2i_p} \end{bmatrix} \tag{35}$$

The constants of integration are denoted B_{11}, B_{12}, ---, B_{1f_p}, B_{2f_p}, and the relationships for the other factors contained in Eq. (35) are the material and structure properties at corresponding mesh points. The Fletcher boundary condition [16] is used at x_j, because it represents the boundary for the complete range of conditions that may exist: from equilibrium (i.e., the photovoltage $V_{Jph} = 0$) through increasing positive values of V_{Jph} up to and including high injection levels where $V_{Jph} \sim V_{bi}$.

In Eq. (33), ΔE_{cj} represents the band edge discontinuity located at the j mesh point. If ΔE_{cj} is positive, the boundary condition describes minority carrier confinement (i.e., electrons confined to the junction region).

The factors ω_{1j} and ω_{2j}, Eq. (14), are the reciprocals of the effective electron diffusion length in the p-type region, and describes the recombination of electrons in the presence of an electric field in the region bounded between the (j-1) and j mesh point. It describes the recombination related to those electrons entering this region across the planes defined by the (j-1) and j mesh points as well as those photoexcited carriers produced by photon absorption within that region. If the electric field, $E_{pj} = 0$, then $\omega_{1j} = -\omega_{2j}$ and are equal in magnitude to the reciprocal of the diffusion length, $L_n = \sqrt{D_n \tau_n}$. Similarly, for degenerate material or for high injection levels, low values of the electric field are obtained, and $\omega_{1j} \simeq -\omega_{2j}$. In both cases, electron drift toward the junction occurs by means of diffusion rather than a combination of diffusion and field-assisted drift. Eq. (10) reduces to the more familiar form to represent photoexcited carriers.

The constants of integration are obtained by solving Eq. (35). While the matrix in Eq. (35) may be inverted to obtain the solution, a recursion relationship exists between the constants of integration. As a result, there is a significant reduction in CPU execution time to obtain the values of these constants through the recursion relationships. For example, in certain iteration procedures, some of the terms in these relationships that depend on geometry and materials properties may not change and need not be calculated for every iteration. There are probably other benefits, which will be revealed as more experience is gained in using this type of modeling program.

The recursion relationships for the constants of integration are given by the following equations:

$$B_{2f_p} \equiv \frac{F_{(2f_p)} - S_n B_{3f_p} (y_{0f_p}) - \sigma_{f_p} \theta_{nf_p} (\delta_{f_p} + S_n)}{\tau_{f_p} (\epsilon_{f_p} + S_n) - \gamma_{nf_p} \sigma_{f_p} (\delta_{f_p} + S_n)} \quad , \tag{36}$$

$$B_{1f_p} \equiv \frac{\tau_{f_p}\theta_{nf_p}(\varepsilon_{f_p}+S_n) - \gamma_{nf_p}[F_{(2f_p)} - S_n B_{3f_p}(y_{0f_p})]}{\tau_{f_p}(\varepsilon_{f_p}+S_n) - \gamma_{nf_p}\sigma_{f_p}(\varepsilon_{f_p}+S_n)} \quad , \tag{37}$$

$$B_{2j} \equiv -\frac{B_{2(j+1)}[\delta_{(j+1)}-\varepsilon_{(j+1)}]+F_{2(j-1)}\delta_{(j+1)}-F_{(2j)}-\sigma_j\theta_{nj}[\delta_{(j+1)}k_{nj}-\delta_j]}{\tau_j[\varepsilon_j-\delta_{(j+1)}k_{nj}]-\gamma_{nj}\sigma_j[\delta_j-\delta_{(j+1)}k_{nj}]} \quad , \tag{38}$$

$$B_{1j} \equiv \theta_{nj}-\gamma_{nj}B_{2j} \quad , \tag{39}$$

$$B_{21} \equiv -\frac{B_{22}(\delta_2-\varepsilon_2)+F_{01}\delta_2-F_{02}-\sigma_1\theta_{n1}(\delta_2 k_{n1}-\delta_1)}{\tau_1(\varepsilon_1-\delta_2 k_{n1})-\gamma_{n1}\sigma_1(\delta_1-\delta_2 k_{n1})} \quad , \tag{40}$$

and

$$B_{11} \equiv \theta_{n1}-\gamma_{n1}B_{21} \quad , \tag{41}$$

There also exists recursion relationships for the θ_{nj}'s and the γ_{nj}'s which are functions of material properties at their assigned mesh points.

Having obtained the constants of integration and substituting them into the relationship representing the appropriate mesh point, there results f_p-relationships which fully describe the behavior of n_{pe} in the p-region. In principle, all device properties may be recovered through the manipulation of n_{pej}s. Using Eqs. (10) and (15) and the corresponding relationships for holes in the n-region, the hole current J_1, Eq. (28), is obtained. Eq. (28) represents a relationship relating photocurrent versus photovoltage. The photovoltaic J-V_{Jph} curve may be obtained from which maximum power and efficiency is calculated. Moreover, the effects on the J-V_{Jph} curve of the phenomena submodels, and material and structure parameters may be investigated through B_{1j}, B_{2j}, and B_{3j}.

SUMMARY

A new computer modeling method is described and is applied to silicon solar cells. The method is similar to numerical integration (NI) methods in that

both require the use of a mesh point field. The set of transport equations is applied to each mesh point, and through a judicious selection of the mesh point distribution, an accurate closed-form analytical function is obtained at the assigned mesh point. Application of the boundary conditions, to an f-mesh point field, results in 2f-equations that require simultaneous solution. This solution is manifested through the determination of the 2f-constants of integration, where each closed-form solution, representing a mesh point, contains two constants of integration. Solar cell transport solution is represented by the complete set of constants of integration obtained in the n- and p-regions. Substituting the constants of integration into the corresponding closed-form analytical function, representing an assigned mesh point, results in a set of analytical functions that is applicable only to its assigned region in the mesh point field. As a result, the complete set of closed-form functions describes the behavior of the photoexcited carrier concentration for a continuum of x-values in the n- and p-regions. The photoexcited carrier relationship is used to obtain the current-voltage relationship, from which the maximum power point and conversion efficiency are determined. Effects of temperature, solar concentration, submodel parameters, and structure parameters may be studied through changes at each mesh point in ω_{1j}, ω_{2j}, B_{1j}, B_{2j}, and B_{3j}.

REFERENCES

1. T. Wada and J. Frey, IEEE Trans. Electron Devices, ED-26, 476-90, 1976.

2. P. Antognetti, Editor: Process and Device Simulation for MOS-VLSI Circuits, S. Selberherr, A. Schiitz, and H. Pötzl, 490, Martinus Nijhoff Publishers, Boston, 1983.

3. T. Wada and J. Frey, "Physical Basis of Short-Channel MESFET Operation," IEEE Trans. Electron Devices, ED-26, 476-90, 1979.

4. J. J. H. Miller, Editor: An Introduction to the Numerical Analysis of Semiconductor Devices and Integrated Circuits, E. M. Buturla, 9-15, Boole Press, Dublin.

5. H. K. Gummel, "A Self-Consistent Iterative Scheme for One-Dimensional Steady-State Transistor Calculations," IEEE Trans. Electron Devices, ED-11, 455-465, 1964.

6. A. DeMari, "An Accurate Numerical Steady-State One-Dimensional Solution of the P-N Junction," Solid-State Electron., 11, 33-58, 1968.

7. A. DeMari, "An Accurate Numerical One-Dimensional Solution of the P-N Junction Under Arbitrary Transient Conditions," Solid-State Electron., 11, 1021-1053, 1968.

8. D. L. Scharfetter and H. K. Gummel, "Large-Signal Analysis of a Silicon Read Diode Oscillator," IEEE Trans. Electron Devices, ED-16, 64-77, 1969.

9. D. P. Kennedy and R. R. O'Brien, "Computer Aided Two-Dimensional Analysis of the Junction Field Effect Transistor," IBM J. Res. Dev., 14, 95-116, 1970.

10. M. Reiser, "A Two-Dimensional Numerical FET Model for DC, AC and Large-Signal Analysis," IEEE Trans. Electron Devices, ED-20, 35-45, 1973.

11. K. Yamaguchi and H. Kodera, "Drain Conductance of Junction Gate FETs in the Hot Electron Range," IEEE Trans. Electron Devices, ED-23, 545-53, 1976.

12. J. L. Gray, "Two-Dimensional Modeling of Silicon Solar Cells," Ph.D. Dissertation, Purdue University, August 1982.

13. D. P. Kennedy and R. R. O'Brien, "Two-Dimensional Mathematical Analysis of a Planar Type Junction Field-Effect Transistor," IBM J. Res. Dev., 13, 662-74, 1969.

14. G. D. Hachtel, M. Mack, and R. R. O'Brien, "Semiconductor Device Analysis via Finite Elements," Eighth Asilomar Conference on Circuits and Systems, Pacific Grove, Calif., 1974.

15. M. F. Lamorte and D. H. Abbott, Final Report No. AFWAL-TR-81-1016: "III-V Detector Modeling," March 1981, WPAFB Contract No. F33615-79-C-1828.

16. N. H. Fletcher, "General Semiconductor Junction Relations," J. Electronics, 2, 609-610, 1957.

DISCUSSION
(LAMORTE)

LINDHOLM: I have a number of small questions. You put your attention on the dependent variables, which you treat as the hole and electron densities. I'm wondering how you enter the external boundary conditions since you are not feeding in hole and electron densities at the ends of the device.

LAMORTE: At the junction side of the end region, for example, meaning the emitter, the boundary condition becomes the Fletcher boundary condition for the photo-excited holes, because we are treating the general case of high injection level. At the surface region we are calculating the recombination velocity, by means of a Δx divided by the lifetime at the center of the first mesh point. And we have gotten some interesting results there, in that it appears that even for calculating the surface recombination velocity in that manner, it may not be consistent with the slope of the photo-excited holes at the surface. If you don't recalculate the surface recombination velocity, the solution will oscillate. We're just putting a fix in that, and the fix is that you want to update the surface recombination velocity at the surface by the exact relationship. Meaning the product of the surface recombination velocity times the photo-excited hole concentration at the surface, and that is equal to the surface recombination current, which includes a drift field component and a diffusion component. So that becomes the left-hand boundary.

LINDHOLM: I have a related question. If you are going to do a non-illuminated analysis where you apply a voltage, then how do you get into the external boundary conditions? I'm not now concerned with the edge of what you call the depletion region but rather the contacts of the device.

LAMORTE: I don't know whether it will work for that, but we can probably make it work. We have not given that any consideration.

LINDHOLM: Would you integrate the electric field? Would that be the way of doing it? Getting integrated, the electric field through the material, and setting that equal to zero, and then you would have to iterate, I suppose.

LAMORTE: Yes, we have that in the model because under high injection level you want to determine what the voltage drop is across the quasi-neutral region.

LINDHOLM: When you say the Fletcher boundary condition, you mean the Fletcher Masawa boundary condition as modified by Houser?

LAMORTE: No, the Fletcher and Masawa conditions are separate. They account for the same thing, but they require different information. The Fletcher boundary condition applies to the edges of the depletion region and thats what we are using. The Masawa uses the right-hand edge of the depletion region and the left-hand contact.

LINDHOLM: How do you define the edge of the depletion region in your numerical analysis?

LAMORTE: We calculate the depletion region for either a graded case or the abrupt case.

LINDHOLM: You calculate it how? Depletion approximation?

LAMORTE: Yes.

LINDHOLM: That won't work, I'm afraid, because you probably need to make a correction because of the free electrons and holes in that region. We could discuss that privately. That is probably an updating of the physics that goes into the model.

LAMORTE: Well, that is updated.

LINDHOLM: Oh, I see. You don't use the depletion approximation to calculate the depletion thickness?

LAMORTE: We use it to get it started.

LINDHOLM: Oh, I see, then you update. Okay. Then how do you define the edge of the depletion region once you get it updated? Somehow you have to use some criterion to define the edge of the depletion region.

LAMORTE: Then we use the depletion approximation.

LINDHOLM: Okay, I don't understand the answer to that, but maybe we could discuss that privately, unless you want to elaborate on it now. What I thought you said was, as your starting point to get the edge of what you call the depletion region, you would use the depletion approximation and then you would iterate up in, including the electron hole densities, in order to redefine the depletion approximation. Then I asked you what the criterion was after you did the updating.

QUESTION: Maybe that's something the two of you could discuss.

LINDHOLM: I have one last question. This is a very interesting idea to me. I have been sounding very negative; I'm sorry to sound negative. I just was looking at some small points. I don't do numerical analysis, but I'm somewhat familiar with what Mike did, and Gummel, and all these other people, and the only place I have ever seen this done previously, similar to this, is in a book by some Russians. I wonder if this is the first time this method has been used?

LAMORTE: I have not seen it anywhere else, and I have spoken to about a dozen people who have done computer modeling in other areas, other than semiconductors, as well, and they claim that they have not seen it. And I have not seen it elsewhere.

LINDHOLM: This Russian book is not quite numerical analysis, so I guess I haven't seen it either, but that's as close as I have come to seeing it.

It's very interesting.

LAMORTE: One of the things that this does for you, and what we showed in the avalanche photo diode -- because you're reflecting a lot of the physics in the closed form solution -- when you look at the convergence of the solution as a function of mesh points, you find that you do not need as many mesh points, for example, in the avalanche photo diode. We didn't need to go above 15 to 20 mesh points when we had a half-micrometer depletion width, and we went all the way up to 80 mesh points, and at 15 to 20 we were within 1% of the asymptotic solution with 80 mesh points. I'm fully convinced that since you have a closed-form solution, which is a good approximation, the physical system, that it's forgiving in terms of using a lesser number of mesh points. And so, therefore, that combined with the recursion formulas, the CPU time is reduced greatly.

LINDHOLM: I was wondering if you could describe the output that you got from your model and do you have it set up to give you graphs of carrier distributions and so forth?

LAMORTE: No, we haven't done that yet. We almost have the model working, meaning that with one of your cells we got something like 38 milliamperes, and it's about 20% too high, so we have gotten it that far and we are still trying to debug and determine where that is. And it may be just a simple matter that the lifetime we are using is too high.

LINDHOLM: So the code doesn't give you plots of carrier distributions and things that help one see what's going on in the physics of the device.

LAMORTE: We get discrete points, for example, of carrier concentration, okay, at the mesh points, and we get it at two points actually, we get it at each of the mesh points and in between. But if you wanted to, by taking the relationship that applies to that particular region of the cell in combination with the appropriate constants of integration, you could plot the entire thing on the continuum if you wished.